Published in final edited form as:

Dev Cell. 2016 September 12; 38(5): 536–547. doi:10.1016/j.devcel.2016.08.001.

PIKfyve regulates vacuole maturation and nutrient recovery following engulfment

Shefali Krishna[1,2], **Wilhelm Palm**[3], **Yongchan Lee**[2], **Wendy Yang**[2], **Urmi Bandyopadhyay**[2], **Haoxing Xu**[4], **Oliver Florey**[5], **Craig B. Thompson**[3], and **Michael Overholtzer**[2]

[1]Gerstner Sloan Kettering Graduate School of Biomedical Sciences, New York, NY 10065, USA

[2]Cell Biology Program, Memorial Sloan Kettering Cancer Center, New York, NY 10065, USA

[3]Cancer Biology and Genetics Program, Memorial Sloan Kettering Cancer Center, New York, NY 10065, USA

[4]Department of Molecular, Cellular, and Developmental Biology, University of Michigan, 3089 National Science Building (Kraus), 830 North University, Ann Arbor, Michigan 48109, USA

[5]Signalling Programme, The Babraham Institute, Cambridge, UK

Summary

The scavenging of extracellular macromolecules by engulfment can sustain cell growth in a nutrient-depleted environment. Engulfed macromolecules are contained within vacuoles that are targeted for lysosome fusion to initiate degradation and nutrient export. We have shown that vacuoles containing engulfed material undergo mTORC1-dependent fission that redistributes degraded cargo back into the endosomal network. Here we identify the lipid kinase PIKfyve as a regulator of an alternative pathway that distributes engulfed contents in support of intracellular macromolecular synthesis during macropinocytosis, entosis, and phagocytosis. We find that PIKfyve regulates vacuole size in part through its downstream effector the cationic transporter TRPML1. Furthermore, PIKfyve promotes recovery of nutrients from vacuoles, suggesting a potential link between PIKfyve activity and lysosomal nutrient export. During nutrient depletion, PIKfyve activity protects Ras-mutant cells from starvation-induced cell death and supports their proliferation. These data identify PIKfyve as a critical regulator of vacuole maturation and nutrient recovery during engulfment.

Graphical Abstract

Correspondence to: Michael Overholtzer, overhom1@mskcc.org.

Author Contributions

S.K. and M.O. designed, carried out experiments and wrote the paper. Y.L. and O.F. performed the *C. elegans* imaging experiments. W.Y. and U.B. contributed experimental assistance and data analysis. W.P. designed and performed the albumin supplementation assays, H.X. contributed reagents, W.P. and C.B.T. assisted in the writing of the manuscript.

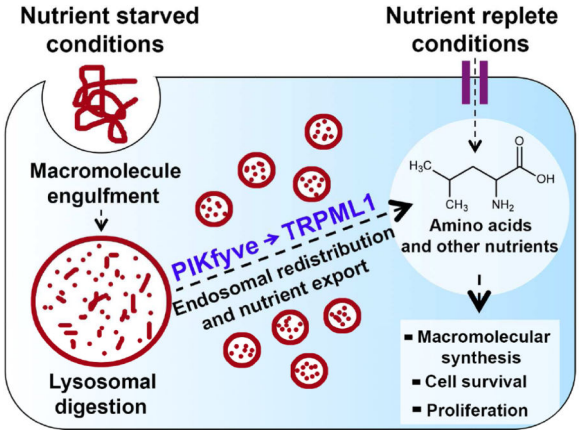

Introduction

Cell proliferation requires bulk production of proteins, lipids and nucleic acids, which places a heavy demand on cellular nutrient and energy supplies. This is particularly true for cancer cells, where normal cell cycle control is often disrupted and proliferation occurs in a dysregulated manner. The rapid expansion of solid tumors often outpaces vascular supply, causing an increased dependence of tumor cells on alternative mechanisms of nutrient acquisition. In addition to cancer cells, non-transformed cells, such as macrophages, neurons, cardiomyocytes, and epithelial and endothelial cells, must also function within ischemic tissues during stroke, heart attack, or injury, or within hypovascular tumor microenvironments, which places a demand on pathways that allow for the scavenging of nutrients needed for cell survival.

One mechanism that supports the recycling of nutrients is macroautophagy (referred to as autophagy), whereby cells sequester intracellular components that undergo lysosomal degradation (He and Klionsky, 2009). Autophagy is induced in ischemic tissues where it has been shown to promote cell survival (Guan et al., 2015; Matsui et al., 2007), although prolonged autophagy can also contribute to cell death in some contexts (Descloux et al., 2015). Certain cancer types, particularly those with mutations in Ras-family small GTPases, also exhibit an elevated level of autophagy that supports cell survival by recycling intracellular macromolecules to maintain mitochondrial function (Guo et al., 2011; Yang et al., 2011). These cancers, demonstrate signs of autophagy “addiction”, where inhibition of autophagy can lead to cell death (Mancias and Kimmelman, 2011).

In addition to autophagy, which utilizes intracellular contents and promotes cell survival, Ras-transformed cells also upregulate mechanisms to scavenge nutrients from the extracellular environment to support proliferation (Commisso et al., 2013; Kamphorst et al., 2013). The engulfment of serum albumin by macropinocytosis can support the proliferation of Ras-mutant cells by supplying exogenous amino acids (Commisso et al., 2013; Palm et al., 2015). Similar to macropinocytosis, engulfment of whole cells by epithelial or cancer cells through entosis, or the engulfment of dead cells by macrophages through phagocytosis, can also provide amino acids that suppress starvation-induced cell death and promote proliferation (Krajcovic et al., 2013). Thus, the ability to scavenge nutrients from

extracellular sources may generally promote the survival and proliferation of different cell types within vascularly compromised environments.

Scavenged macromolecules are contained within vacuoles that are targeted for fusion with lysosomes to initiate cargo degradation and nutrient export (Fairn and Grinstein, 2012; Kinchen and Ravichandran, 2008; Racoosin and Swanson, 1993). We have shown that maturation of macroendocytic vacuoles after lysosome fusion involves membrane fission that shrinks their size as engulfed material is degraded. At least one mechanism of vacuole shrinkage has been shown to be regulated by the amino acid-responsive mTORC1 protein kinase that localizes to vacuole membranes, and results in redistribution of engulfed material throughout the endosome/lysosome network (Krajcovic et al., 2013). Whether this is the sole fate of lysosomally degraded extracellular macromolecules remains unknown.

In order to explore further how the contents of macroendocytic vacuoles are processed and utilized, we sought to identify other regulators of vacuole dynamics. For example, mTORC1 activity and localization has been shown to be regulated by PIKfyve, a lipid kinase that converts PI(3)P into PI(3,5)P2 in the endocytic pathway (Bridges et al., 2012; Sbrissa et al., 1999). Since PIKfyve loss-of-function is known to lead to enlargement of late endosomal/lysosomal vesicles (Ikonomov et al., 2001; Nicot et al., 2006; Shisheva, 2001), we investigated the possibility that PIKfyve may play a role in regulating the redistribution and cytosolic uptake of nutrients that accumulate in lysosomes following degradation of engulfed cells and macromolecules.

Results

PIKfyve regulates entotic vacuole, phagosome and macropinosome shrinkage *in vitro* and *in vivo*

As PIKfyve is reported to maintain lysosome morphology and support mTORC1 activity, we hypothesized that it might regulate the redistribution of the contents of large lysosomal vacuoles that are formed during cell engulfment. To investigate if PIKfyve contributes to resolving the large lysosomal vacuoles that form as a result of the live cell engulfment mechanism entosis, we treated cells with two inhibitors of PIKfyve kinase activity, YM201636 (YM201) (Jefferies et al., 2008) and Apilimod (Cai et al., 2013), and monitored the size of entotic vacuoles through time using H2B-mCherry fluorescence derived from engulfed cells, as we reported previously (Krajcovic et al., 2013). Whereas entotic vacuoles in vehicle-treated MCF10A or HEK-293 cells reduced in size over time as cell corpses were degraded, vacuoles within PIKfyve-inhibited cells failed to shrink over 20 hours, despite the degradation of corpses observed by DIC imaging (Figure 1A,B, Figure S1A, Movie S1). Likewise, the knockdown of PIKfyve expression with two independent shRNAs also slowed vacuole shrinkage (Figure 1C). Together, these data indicate a role for PIKfyve in this late stage of vacuole maturation. We also quantified the presence of mCherry-positive vesicles in the cytoplasm of corpse-containing cells, which we have measured previously as a readout of membrane fission (Krajcovic et al., 2013). PIKfyve inhibition significantly reduced the percentage of cells accumulating mCherry vesicles, suggesting that PIKfyve is required in part to initiate the redistribution of accumulated lysosomal contents back into the endosome network (Figure S1B,C).

We next sought to determine if PIKfyve might play a similar role to regulate the resolution of large lysosomal compartments resulting from apoptotic cell phagocytosis. We examined phagosomes in J774.1 macrophages incubated with H2B–mCherry labeled apoptotic corpses. Like entotic vacuoles, apoptotic corpse-containing phagosomes in PIKfyve-inhibited cells exhibited decreased rates of vacuole shrinkage compared to controls, despite the degradation of ingested apoptotic corpses (Figure 1D,E). To further extend these findings to an *in vivo* system, we examined the requirement of the PIKfyve ortholog *ppk-3* for apoptotic phagosome shrinkage during *C. elegans* embryogenesis, where phagocytosis is well known to clear cells that undergo developmentally programmed apoptosis. Using *C. elegans* embryos co-expressing H2B::mCherry and PIP2::GFP in strain *OD95* (Green et al., 2011; McNally et al., 2006), we quantified the shrinkage of phagosomes (indicated by mCherry fluorescence), after the completion of engulfment (indicated by loss of PIP2::GFP from phagosome membranes) (Figure 1F). Consistent with our *in vitro* studies, *ppk-3* mutant embryos (Nicot et al., 2006) showed significantly decreased rates of phagosome shrinkage compared to wild-type embryos (Figure 1G).

Finally, to investigate if PIKfyve also regulates macropinosome maturation, we monitored macropinosomes in macrophages incubated with fluorescent dextran by time lapse-imaging. Nascent macropinosomes were observed to undergo fusion with lysosomes (as measured by co-staining with lysotracker) and then rapidly shrink in size over time (Figure S1D,E, Movie S2). The inhibition of PIKfyve blocked the ability of macropinosomes to shrink after lysosome fusion, consistent with the function of PIKfyve in vacuole shrinkage during entosis and phagocytosis (Figure S1D,E, Movie S3). We further observed transient recruitment of PIKfyve-eGFP onto macropinosomes as they underwent shrinkage in HEK293 cells (Figure S1F,G). PIKfyve inhibition by treatment with YM201 prolonged the association of PIKfyve with macropinosomes, whose sizes remained unchanged over time (Figure S1F,G). Taken together, these data demonstrate that PIKfyve controls the maturation of entotic vacuoles, phagosomes and macropinosomes, by functioning at a post-lysosome fusion stage in the degradation of extracellular material.

PIKfyve controls vacuole shrinkage independent of upstream endocytic functions

As PIKfyve has been suggested to play various roles in lysosome physiology (de Lartigue et al., 2009; Ikonomov et al., 2001, 2006; Jefferies et al., 2008; Kerr et al., 2010; Kim et al., 2014; Nicot et al., 2006; Rusten et al., 2006; Sbrissa et al., 2007), we next examined if PIKfyve might also regulate earlier steps in delivery of extracellular cargo to lysosomes. During entotic cell death, the endosomes containing engulfed cells undergo sequential steps of maturation involving phosphorylation of phosphatidylinositol to form phosphatidylinositol-3-phosphate, lipidation of autophagy protein LC3, and recruitment of late endosomal marker Rab-7, all of which appeared unperturbed by PIKfyve inhibition (Figure S2A,B). During entosis, these upstream maturation events are important for the fusion of lysosomes to entotic vacuoles, which triggers the death of internalized cells (Florey et al., 2011). We found that recruitment of the lysosomal marker Lamp1 (Figure S2B), and the rate of entotic cell death (Figure S2C) were not significantly altered by PIKfyve inhibition, consistent with normal upstream vesicle-to-lysosome maturation. We also noted by DIC imaging that PIKfyve-inhibited cells appeared to degrade entotic cell corpses with

kinetics similar to control cells, even though the large vacuoles failed to undergo fission (Figure 1A, Movie S1).

To examine the effects of PIKfyve inhibition during apoptotic corpse engulfment in macrophages, we investigated acidification and cathepsin protease activity through lysotracker and DQ-BSA staining. Apoptotic phagosomes showed lysotracker and DQ-BSA-positive staining in both control and PIKfyve-inhibited macrophages, consistent with normal acidification and degradative capacity (Figure S2D). In contrast, treating cells with the acidification inhibitor Concanamycin A effectively prevented lysotracker and DQ-BSA staining (Figure S2D). To further monitor the phagocytic engulfment and degradation of apoptotic cells by macrophages, we examined the accumulation of corpse-derived mCherry protein, which is generated by the degradation of ingested H2B-mCherry-expressing apoptotic cells (Krajcovic et al., 2013). mCherry accumulation occurred with similar kinetics in control and PIKfyve-inhibited cells, but was blocked by Concanamycin A (Figure S2E), consistent with normal phagocytosis and lysosomal degradation of apoptotic cells in PIKfyve-inhibited macrophages.

To further address the role of PIKfyve in an experimental system where corpse degradation can be bypassed (Krajcovic et al., 2013), we blocked entotic vacuole shrinkage by treating nutrient-replete cells with the mTOR kinase inhibitor Torin1, until engulfed cell corpses were visibly digested as determined by DIC microscopy (after 16 hours), but vacuoles were still large and intact. We then washed out Torin1 and observed the vacuolar dynamics in the presence or absence of PIKfyve inhibition. While control vacuoles underwent rapid shrinkage after Torin1 washout, PIKfyve inhibition significantly delayed shrinkage (Figure S3A,B). Altogether these data support a model where PIKfyve regulates the ability of cells to clear large lysosomal vacuoles independently of the ability of lysosomal proteases to degrade engulfed material.

PIKfyve regulates vacuole shrinkage through TRPML1 in an mTORC1-independent manner

We next examined how PIKfyve regulates vacuole shrinkage by interrogating potential downstream effectors. Given the reported role of PIKfyve in supporting mTORC1 activity, and the role of mTORC1 in lysosome fission, we determined the effects of PIKfyve inhibition on mTORC1 activity and localization (Bridges et al., 2012). Both MCF10A cells and J774.1 macrophages cultured in amino acid-free media or treated with Torin1 showed a loss of mTORC1 activity, as monitored by threonine 389 phosphorylation of its downstream target, S6-ribosomal protein kinase (pS6K) (Figure 2A, Figure S3C). In contrast, when PIKfyve was inhibited, both cell types exhibited normal pS6K levels in nutrient-replete media (Figure 2A, Figure S3C). PIKfyve inhibition also had no effect on the reactivation of mTORC1 by amino acids in starved cells (Figure 2B, Figure S3D). We have shown previously that mTOR localizes to corpse-containing lysosomal compartments (Krajcovic et al., 2013), and mTOR co-localization to entotic vacuoles and phagosomes was also unaffected by PIKfyve inhibition (Figure 2C, Figure S3E). These data suggest that PIKfyve does not function upstream of mTORC1 to regulate vacuole shrinkage.

Since PIKfyve was not regulating mTORC1 in our cell systems, we examined the potential role of another PIKfyve effector, the lysosomal cation channel TRPML1/MCOLN1.

TRPML1 has been shown to bind PI(3,5)P2, the lipid product of PIKfyve, to regulate lysosome function, and its mutation underlies the lysosome storage disorder Mucolipidosis IV (Dong et al., 2010; Sun et al., 2000). To examine the role of TRPML1 in vacuole shrinkage, we utilized a previously reported pharmacological inhibitor ML-SI3(Samie et al., 2013) to acutely inhibit TRPML-1 function. As shown in Figure 2D, treatment of cells with ML-SI3 significantly delayed the shrinkage of macropinosomes, demonstrating that TRPML-1 is required for macropinosome maturation in a similar manner to PIKfyve. We also generated shRNA-mediated knockdowns of TRPML1, which led to a slight but reproducible delay in vacuole shrinkage during entosis (Figure S3F,G). However, TRPML1 shRNA also affected corpse degradation (data not shown), suggesting that TRPML1 could be required for general lysosome function. In order to further examine a role for TRPML1 downstream of PIKfyve in regulating vacuole shrinkage, we hypothesized that overexpressing the channel might rescue the effects of PIKfyve inhibition, similar to what has been shown for other endosomal compartments (Dong et al., 2010). Indeed, upon treatment with PIKfyve inhibitors, vacuole shrinkage was rescued in cells overexpressing TRPML1-eGFP, but not in adjacent, non-expressing control cells (Figure 2E,F, Movie S4). Interestingly, TRPML1 overexpression had no effect on Torin1-induced increase in vacuole size, (Figure 2F), supporting a model that TRPML1 and mTORC1 function in an independent pathway of resolving large lysosomal vacuoles that have accumulated extracellular macromolecules.

Lysosomal cation fluxes regulate vacuole fission downstream of PIKfyve

The regulation of vacuole maturation by PIKfyve and its effector ion channel TRPML-1 led us to consider that lysosomal ion fluxes may be linked to vacuole fission regulated by PIKfyve. As TRPML-1 is a known cation channel that can efflux calcium, we treated cells with an inhibitor of calcium signaling at lysosomes, *trans*-Ned 19, which is an NAADP antagonist. NAADP signaling mobilizes calcium release from lysosomal cation channels including TRPML1, and *trans*-Ned 19 has been shown to block calcium release from lysosomes (Lee et al., 2015). Consistent with TRPML1 loss-of-function, *trans*-Ned 19 induced a significant delay in entotic vacuole shrinkage (Figure 3A), but also delayed corpse degradation (data not shown). To examine if *trans*-Ned 19 could affect vacuole shrinkage independent of upstream degradation events, we performed a washout experiment where we blocked vacuole shrinkage by inhibiting PIKfyve with YM201, until engulfed cell corpses were visibly digested as determined DIC microscopy (after 16 hours), but the vacuoles were still large and intact. We then washed out YM201 and observed the vacuolar dynamics in the presence or absence of *trans*-Ned 19. While control vacuoles underwent rapid shrinkage after YM201 washout, *trans*-Ned 19 treated vacuoles showed significantly delayed shrinkage (Figure 3B). These data suggest a role for NAADP-dependent calcium signaling at lysosomes in redistribution of lysosomally accumulated material downstream of PIKfyve activity.

The effect of lysosomal calcium efflux could suggest a role for increased cytosolic calcium concentrations in vacuole shrinkage. To test this, we increased cellular calcium levels by treatment with calcium ionophore Ionomycin, but this did not rescue the effects of PIKfyve inhibition on vacuole shrinkage (Figure 3C), suggesting that the block in fission resulting

from inhibition of PIKfyve may not be due to an inhibition of cytosolic calcium signaling. Alternatively, we reasoned that calcium efflux could function to reduce the high ionic burden generated by engulfed extracellular material in vacuoles. We therefore considered that PIKfyve inhibition may inhibit vacuole shrinkage at least in part by limiting cation efflux, resulting in hyperosmotic stress in the vacuoles. Hence, in order to determine if manipulation of ionic balances could affect vacuole size, we first pre-treated cells with YM201 to generate large entotic vacuoles. We then examined the effects of hypertonic or hypotonic medium, which would induce vacuolar efflux or influx of water(Florey et al., 2015), on vacuole shrinkage. Indeed, while vacuoles in YM201-treated cells did not shrink (Figure 3D upper panel, 3E, Movie S5), vacuoles in YM201 treated cells cultured in hypertonic medium underwent rapid shrinkage associated with the appearance of mCherry vesicles in the cytoplasm (Figure 3D lower panel, 3E, Movie S5). Conversely, while vacuoles shrank normally after the washout of YM201, treatment with hypotonic medium was sufficient to completely prevent vacuole shrinkage (Figure 3E). These data suggest a role for the efflux of lysosomal cations downstream of PIKfyve and TRPML1 in controlling vacuole shrinkage.

PIKfyve-mediated maturation regulates nutrient recovery from phagosomes

We have reported previously that nutrients recovered from engulfed corpses can support cell survival and proliferation during starvation (Krajcovic et al., 2013). To determine if amino acid export from phagosomes required PIKfyve activity, we quantified the incorporation of radiolabeled amino acids from phagocytosed apoptotic corpses into GFP synthesized by macrophages, an assay we published previously to quantify nutrient recovery (Krajcovic et al., 2013). As shown in Figure 4A, PIKfyve inhibition reduced the amount of radiolabeled amino acid incorporation, but had no effect on engulfment or degradation, as evidenced by similar levels of mCherry protein derived from ingested and degraded apoptotic cells, consistent with the regulation of nutrient recovery by PIKfyve. To further examine if PIKfyve activity was required for the utilization of engulfed nutrients, we investigated amino acid signaling and cell proliferation in control and PIKfyve-inhibited cultures. We have shown that nutrient recovery from phagosomes reactivates mTORC1 under starvation conditions, as monitored by restoration of pS6K levels when macrophages cultured in amino acid-free media are fed with apoptotic corpses (Krajcovic et al., 2013). While PIKfyve had no effect on mTORC1 activity when stimulated by free amino acids (Figure 2B, Figure S3D), PIKfyve inhibition was able to block mTORC1 reactivation when amino acids were supplied in the form of engulfed apoptotic corpses (Figure 4B), consistent with defective lysosomal amino acid export. Finally, as J774.1 macrophages are a proliferative cell line, we further examined the ability of apoptotic corpses to support J774.1 macrophage proliferation by quantifying fold changes in cell number over time in starved and corpse-fed cultures. As shown in Figure 4C,D, feeding macrophages with apoptotic cell corpses under amino acid-free conditions supported proliferation in PIKfyve-dependent manner. Taken together, these data support a model that PIKfyve is required for the recovery of nutrients from phagosomes in macrophages.

PIKfyve is required for albumin-dependent growth of Ras-transformed cells

It has been reported recently that Ras-transformed cells utilize macropinocytosis of albumin to support their growth under nutrient-deprived conditions (Commisso et al., 2013). We hypothesized that PIKfyve might regulate nutrient recovery during this process, similar to its function during apoptotic cell phagocytosis. To examine the effect of PIKfyve inhibition on cell proliferation that is dependent on macropinocytosis, we took advantage of a recently published system that allows cells to grow utilizing extracellular proteins. K-Ras G12D knock-in mouse embryo fibroblasts (MEFs) are unable to proliferate during leucine depletion, but cell proliferation is restored by supplementing medium with 3% BSA (Palm et al., 2015). By using this system, we found that treatment with the PIKfyve inhibitors Apilimod and YM201 abolished the BSA-dependent rescue of proliferation of cells cultured in leucine-free media (Figure 5A, Figure S4A). It has been shown that mTOR inhibition by treatment with Torin1 actually increases the growth of K-Ras G12D MEFs during starvation due to increased lysosomal degradation of BSA (Palm et al., 2015). We also found that the inhibition of PIKfyve abolished the Torin1-dependent increase in proliferation (Figure 5A). Importantly, PIKfyve inhibition had no effect on the uptake and degradation of BSA, as evidenced by DQ-BSA fluorescence that was similar between control and Apilimod-treated cells, but strongly decreased when cells were treated with lysosomal protease inhibitors (Figure 5B, Figure S4B,C). Similar to the inhibition of PIKfyve with pharmacological agents, the siRNA-mediated knockdown of PIKfyve expression also inhibited albumin-dependent growth of K-Ras G12D MEFs, while having no effect in nutrient-replete conditions (Figure 5C,D, Figure S4D). We further examined the BSA-mediated growth of tumor cells derived from a Kras-mutant mouse model of pancreatic cancer KRPC (Lito et al., 2014), and human cancer cells MiaPaca-2 (pancreatic cancer, Kras mutant) and T24 (bladder cancer, H-Ras mutant). PIKfyve inhibition consistently blocked cell proliferation when starvation media were supplemented with 3% BSA (Figure 5E–G), while having no effect in full media conditions (Figure S4E–H), demonstrating that PIKfyve is required for albumin-dependent growth of Ras-mutant cancer cells.

Discussion

The data presented here establish that PIKfyve controls a late stage of macroendocytic vacuole maturation, involving redistribution of engulfed cargo to lysosome networks. While a role for PIKfyve in regulating lysosome morphology has been established previously (Ikonomov et al., 2001; Nicot et al., 2006; Rudge et al., 2004), mechanistic studies have suggested conflicting functions of PIKfyve in maintaining lysosomal pH, supporting proteolytic degradation, or promoting lysosome fusion (de Lartigue et al., 2009; Ho et al., 2015; Ikonomov et al., 2001, 2006; Jefferies et al., 2008; Kerr et al., 2010; Kim et al., 2014; Nicot et al., 2006; Rusten et al., 2006; Sbrissa et al., 2007). Recent studies have also concluded that PIKfyve is required for engulfment by phagocytosis, phagolysosome formation and cargo degradation (Dong et al., 2010; Kim et al., 2014). Although we cannot completely rule out upstream functions, we find here that PIKfyve is not required for the engulfment or degradation of apoptotic corpses during phagocytosis by macrophages, or during *C. elegans* embryogenesis *in vivo*. Further, the ingestion and degradation of serum albumin by macropinocytosis is unaffected by PIKfyve inhibition. Our findings instead

implicate PIKfyve in controlling the ability of the cell to clear large lysosomal vacuoles and redistribute their contents. It is conceivable that the different substrates used for engulfment between our study and others (Dong et al., 2010; Kim et al., 2014) could account for some of the observed effects, as we note that latex beads used as phagocytosis substrates cannot be degraded and redistributed by uptake into the cytosol.

Although previous studies have shown that both PIKfyve and TRPML1 can regulate mTORC1 (Bridges et al., 2012; Wong et al., 2012), we found that PIKfyve functions largely independently of mTORC1 to control vacuole shrinkage. PIKfyve activity was required for mTORC1 activation in our systems only under conditions when cells are dependent on nutrients supplied by engulfment, an effect we speculate may be due to reduced nutrient recovery from macroendocytic vacuoles upon PIKfyve inhibition. We find evidence instead that PIKfyve may control vacuole shrinkage at least in part through its effector, the Ca2+ channel TRPML1, as its inhibition slows vacuole shrinkage in a similar manner to PIKfyve inhibition, and shrinkage is rescued in PIKfyve-inhibited cells by TRPML1 overexpression. Perhaps consistent with this model, altering the ion balance by placing cells in hypertonic conditions restores vacuole shrinkage in PIKfyve-inhibited cells, suggesting a link between PIKfyve activity and osmotic regulation in controlling vacuolar dynamics, although a more general effect of hypertonicity cannot be excluded. Interestingly, TRPML1 overexpression does not rescue vacuole shrinkage induced by mTOR inhibition, consistent with PIKfyve and mTORC1 controlling vacuolar shrinkage through separate pathways. While we find that PIKfyve is not required for the degradation of engulfed corpses, TRPML1 loss of function does slow corpse degradation (data not shown), similar to a recent report (Dayam et al., 2015), suggesting that TRPML1 has PIKfyve-independent upstream functions. Perhaps basal ion fluxes controlled by TRPML1 are generally required to maintain lysosome function and further TRPML1 activation by PIKfyve is required to support the shrinkage of macroendocytic vacuoles that harbor complex substrates undergoing degradation, which is predicted to alter their osmotic potential. The molecular mechanism underlying how osmotic changes may influence vacuolar dynamics, and the source of luminal ions potentially effluxed by TRPML1 in this context, remain to be elucidated by further studies. We note that the removal of calcium from culture medium does not appear to affect the shrinkage of macropinosomes (Figure S5A), suggesting that lysosomal calcium originating from sources other than engulfed substrates could also contribute. One such potential source is the endoplasmic reticulum, which has been implicated in maintaining lysosomal calcium that is effluxed by TRPML1 (Garrity et al., 2016). Examining the kinetics of TRPML1-dependent calcium flux using calcium sensors may be informative, but overlaying potentially transient currents with the longer timescale of vacuole shrinkage has proved technically challenging. Future studies may elucidate the kinetics of TRPML1-mediated ion movements in this context. It is also important to point out that while we favor a model that TRPML1 may function as an effector of PIKfyve in this context, our data do not exclude a parallel relationship, or that PIKfyve could affect redistribution of vacuolar contents through additional downstream effectors. We have examined two other known PI(3,5)P2 effectors,WIPI-1, WIPI-2, and have not found a requirement for vacuole shrinkage by loss-of-function approaches (data not shown).

In addition to supporting vacuole shrinkage, we also find that PIKfyve facilitates the utilization of nutrients from engulfed substrates, suggesting a potential link between shrinkage and nutrient export, which could occur by several mechanisms. The role of calcium and hypertonicity in the resolution of large vacuoles may suggest that ion transport may directly facilitate the cytosolic uptake of amino acids in the lysosome. Alternatively, the redistribution of degraded cargo from large vacuoles into the entire lysosome network alters the surface area-to-volume ratio, which could contribute to enhanced export. Perhaps analogously, starvation is known to increase the absorptive surface area of intestinal epithelial cells by 2–3-fold, in order to maximize nutrient uptake from the intestinal lumen (Gupta and Waheed, 1992). The fission of large macroendocytic vacuoles is predicted to increase surface area-to-volume by at least 10-fold (Figure S5B), and may therefore increase the efficiency of nutrient export significantly. Finally, it is also possible that PIKfyve controls nutrient export more directly by supporting the activity of amino acid and other nutrient transporters whose identities remain poorly characterized.

Our findings demonstrate that PIKfyve is required for Ras-mutant cells to scavenge nutrients by macropinocytosis. Ras-mutant cells show an increased dependence on nutrient recovery by macropinocytosis during starvation to satisfy their high metabolic demand (Commisso et al., 2013). This could be of particular importance for pancreatic cancers (>90% have Kras mutations) that are known to be nutrient-deprived due to limited vascularization (Hidalgo, 2010). Since both autophagy and macropinocytosis require lysosome function for nutrient recovery, the use of lysosome inhibitors for pancreatic cancer may hold therapeutic potential. Our data identify PIKfyve as a potential therapeutic target, as its inhibition blocks the ability of Ras-mutant cells to scavenge nutrients by inhibiting vacuole shrinkage and nutrient export. PIKfyve inhibition has minimal effects on the proliferation of control cells and of Ras-mutant cells in nutrient-replete media, suggesting this strategy could specifically target tumor cells in a nutrient-poor microenvironment. Given that the PIKfyve inhibitor Apilimod is currently in clinical trials for autoimmune disorders and is well tolerated in patients (Burakoff et al., 2006; Krausz et al., 2012), this drug may have potential therapeutic value for patients with Ras-driven cancers.

It is interesting to note that while mTORC1 and PIKfyve both regulate the shrinkage of macroendocytic vacuoles, their inhibition has opposing effects on albumin-mediated rescue of cells harboring oncogenic Kras mutations. mTORC1 inhibition has been shown to increase cell proliferation during starvation by upregulating lysosomal degradation of engulfed albumin (Palm et al., 2015). During Kras-driven pancreatic tumorigenesis *in vivo*, mTORC1 inhibition enhances tumor cell proliferation in the central, nutrient-deprived regions while inhibiting proliferation at the nutrient-replete tumor edges (Palm et al., 2015). Our data demonstrate that PIKfyve inhibition can block the proliferation of starved Ras-mutant cells even when they are mTORC1-inhibited, suggesting that a combined strategy of mTORC1 and PIKfyve inhibition may be an approach to limit proliferation in both nutrient-replete and nutrient-deprived regions of cancers.

Experimental Procedures

Cell culture and Reagents

MCF10A cells were obtained from American Type Culture Collection (ATCC, Manassas, VA) and cultured as described (Florey et al., 2011). J774.1 mouse macrophages (ATCC), EL4 cells (kind gift from Dr. Julie Blander, Mt Sinai Hospital, NY), HEK293 (ATCC), Kras G12D Mouse Embryonic Fibroblasts (MEFs) (kind gift from Dr. Scott Lowe, MSKCC, NY), KRPC (Lito et al., 2014), MiaPaca2 (ATCC) and T24 (ATCC) cells were cultured in DMEM plus 10% heat-inactivated fetal bovine serum (FBS) with penicillin/streptomycin (pen/strep). U937 cells (ATCC) were cultured in RPMI-1640 medium plus 10% FBS and pen/strep. Amino acid–free medium was prepared by dialyzing heat-inactivated FBS (for J774.1) or horse serum (for MCF10A) as described (Krajcovic et al., 2013) and adding to amino acid-free base media at 10% final. Hypertonic and hypotonic medium were prepared by addition of 200mM sucrose or 60% water to full growth media respectively. Calcium-free media was prepared by adding dialyzed heat-inactivated FBS to calcium free DMEM (21068028, Thermo Fisher Scientific, USA), and calcium replete media was prepared by addition of 1.8mM calcium to the calcium-free media. MCF10A, HEK293 or U937 cells expressing H2B-mCherry, 2xFYVE-mCherry or GFP-LC3 were prepared by retroviral transduction with pBabe-H2B-mCherry, 2XFYVE-mCherry (FYVE domain from Hrs) and pBabe-GFP-LC3 respectively. Cells were treated with YM201636 (524611, Calbiochem, EMD Millipore, Massachusetts) at 0.4μM for MCF10A cells, 0.8μM for HEK293 cells and 0.8μM-1μM for J774.1 cells, Apilimod (STA5326, Axon1369, Axon Medchem, Netherlands) at 0.1μM, ML-SI3 at 50 μM Torinl (Tocris Bioscience, Bristol, UK) at 0.5μM, *trans-Ned* 19 at 250μM, lonomycin at 1μM, Concanamycin A (Sigma) at 0.1 μM and protease inhibitors at 2 μM E-64, 2 μM Pepstatin A and 10 μM Leupeptin unless otherwise indicated. Cells were treated with lysotracker Green DND-26 (Invitrogen) at 50nM, 10kD-70kD TMR-Dextran (Invitrogen) at 250μg/ml and DQ-BSA Green (Invitrogen) at 10μg/ml.

Constructs and cDNA Transfection

1×10^6 MCF10A–H2B–mCherry cells were nucleofected with TRPML1-eGFP with Amaxa Nucleofector Solution V (Lonza, Switzerland) and assayed 72h post-transfection. 1×10^6 HEK293 cells were plated in 6-well plates, transfected with 4ug PIKfyve-eGFP construct using Lipofectamine 2000 the next day and assayed 48h post-transfection. The pEGFPC1-TRPML1 construct was a kind gift from Dr. Shmuel Muallem, NIH, Bethesda, MD. PIKfyve-eGFP constructs were a kind gift from Dr. Frederic Meunier, University of Queensland, Australia and Dr. Assia Shisheva, Wayne State University, Mi.

Measuring vacuole shrinkage by time-lapse microscopy

To quantify vacuole shrinkage, cells were plated on glass-bottom 6-well plates (MatTek, Ashland, MA) and imaged the next day in 37”C and 5% CO_2 live-cell incubation chambers, as described (Krajcovic et al., 2013). Differential Interference Contrast (DIC) and fluorescence images were obtained every 15 minutes for 24–48 hours. Area of entotic vacuoles and phagosomes were determined by mCherry fluorescence and quantified manually using Elements software. The time point of mCherry protein diffusion from the

nucleus of the corpse to the vacuole during entosis or phagocytosis was determined to be the time zero, and vacuole area was quantified at 10h and 4h respectively as described (Krajcovic et al., 2013). Cell fates of internalized cells were quantified as entotic death, release, no change, apoptosis and proliferation.

Measuring macropinosome shrinkage by confocal microscopy

J774.1 macrophages were cultured on 35mm glass-bottomed dishes (MatTek, Ashland, MA) in full medium with 200 U/ml interferon-y for 48 h, or transfected HEK293 cells were cultured on 35mm glass-bottomed dishes and imaged at 37°C and 5% CO_2 live-cell incubation chambers with 10–70kD Texas-Red Dextran (0.1mg/ml) and lysotracker green (50nM, Invitrogen) added to the media. DIC and fluorescent images were acquired in 0.5μm z-steps, at maximum speed, using the Ultraview Vox spinning-disk confocal system (Perkin Elmer) coupled to a Nikon Ti-E microscope as described(Krajcovic et al., 2013). The time points where dextran macropinosomes became positive for lysotracker staining were considered to be time zero. In J774.1 macrophages, macropinosome areas were quantified at time zero and 30min manually using Volocity software, for the z-planes with maximum area.

Imaging *C. elegans* apoptotic phagocytosis

The H2B::mCherry and PIP2::GFP expressing *ppk3* mutant was generated by crossing the H2B::mCherry and PIP2::GFP expressing OD95 strain with *ppk3 n2668* mutant strain (AC257). Both strains were obtained from the *Caenorhabditis* Genetics Center (University of Minnesota, Minneapolis, MN). Embryos at the 100-cell stage obtained from dissected gravid hermaphrodites were imaged by confocal microscopy as described (Florey et al., 2011). DIC and fluorescent images of the engulfment of apoptotic corpse (ABplpappap) by neighboring cell (ABplpappaa) at 1μm z-stacks were acquired every 4min. The time point of mCherry protein diffusion from the nucleus of the apoptotic corpse to the vacuole was determined to be the time zero, and vacuole area was quantified at 30min.

Western Blotting

Cell Lysis was performed in ice-cold RIPA buffer, followed by SDS-PAGE and western blotting, using Anti-PIKfyve (ab137907; Abeam), anti–S6-Kinase (9202; Cell Signaling), anti-phospho-S6-kinase threonine 389 (9234; Cell Signaling), anti-actin (A1978; Sigma), anti-mCherry (ab125096; Abeam) antibodies, and anti-GFP (11814460001; Roche).

Immunofluorescence

Immunofluorescence was performed on cells cultured on glass-bottom dishes (MatTek) as described previously (Overholtzer et al., 2007). Cells were fixed in 1:1 chilled Methanol:Acetone at −2°C for 5 minutes. The antibodies used for IF were anti-mTOR (2983; Cell Signaling), anti-Lamp1 (for MCF10A cells; BD555798), anti-Lam p1 (for J774.1 mouse macrophages; BD553792), and anti-Rab7 (9367; Cell Signaling, Danvers, MA). Confocal microscopy was performed using the Ultraview Vox spinning-disk confocal system (Perkin Elmer, Waltham, MA) to acquire Z-stack images using Volocity software (Perkin Elmer).

RNAi

1×10^5 MCF10A cells were seeded per well in a six-well plate, followed by lentiviral transduction with control empty LKO.1 vector or the targeted hairpin vectors against PIKfyve or TRPML1. After 48 hours of transduction, cells expressing the shRNAs were selected using puromycin (2μg/ml) and assayed. siGenome SMART pool siRNAs against mouse *PIKfyve*, and Control 2 non-targeting siRNAs, were obtained from Dharmacon. 2×10^5 MEF cells were seeded per well in six-well plate, followed by lipofectamine (Invitrogen) transfection with 250nM control or targeted siRNA against PIKfyve for 6 hours. After 24 hours of transfection, cells were subject to BSA supplementation assays.

Quantitative PCR

Total RNA was extracted from shRNA expressing cells using TRIzol® Plus RNA Purification Kit (12183-555, Thermo Fisher Scientific, USA). Quantitative PCR was performed using the Bio-Rad iCycler real-time system (MyiQ), with SYBR green detection (iScript One-Step RT-PCR Kit with SYBR green (Bio-Rad). Samples were analyzed by the standard curve method in triplicate. Primers against *TRPML1* (QT00094234), *GAPDH* (QT01192646), *mPIKfyve* (QT00127799) and *mGAPDH* (QT01658692) were obtained from Qiagen.

Phagocytosis & Crystal Violet Assays

We plated 1×10^5 J774.1 mouse macrophages onto six well tissue culture plastic plates and cultured them in full medium with 200 U/ml interferon-y for 48 h. After 48hours, cells were washed three times in PBS and fed with 2×10^6 apoptotic cell corpses in amino acid free media for western blotting or serum and amino acid free media for crystal violet (CV) assays. Apoptotic corpses were prepared by UV irradiation of U937 cells expressing H2B-mCherry for western blotting, and EL4 cells for CV assays by overnight incubation and harvesting by centrifugation. 48h after addition of corpses, macrophages were washed three times in PBS and lysed for western blotting or fixed with 4% paraformaldehyde for CV. Fixed cells were stained with 0.1% Crystal Violet Solution and dried overnight before taking images of the plates using the Optronix Gelcount colony counter (Oxford Optronix Ltd., Oxford, UK). The crystals were dissolved in 10% acetic acid and the absorbance at 590nm quantified using spectrophotometry. 35S–Cysteine/Methionine radiolabeling assay was conducted as described previously (Krajcovic et al., 2013).

Lysotracker and DQ-BSA Imaging

J774.1 mouse macrophages were plated on glass-bottom dishes and cultured them in full medium with 200 U/ml interferon-γ for 48 h and pretreated with vehicle or inhibitors for one hour. LysoTracker or DQ-BSA staining was performed by adding 50 nM LysoTracker Green (Invitrogen, Carlsbad, CA) or 0.1mg/ml DQ-BSA (Invitrogen, Carlsbad, CA) to culture media for 30 min before imaging live cells using confocal and time-lapse microscopy.

BSA supplementation Assays

Cell Proliferation assays in full medium or in leucine-free media with or without BSA supplementation were performed in Kras G12D MEFs, KRPC, MiaPaca-2 and T24 cell lines as described (Palm et al., 2015). Fold change in cell number from day 0 to day 4 for leucine-free conditions, and day 0 to day 2 for leucine-replete conditions was quantified.

Statistics and Representative Figures

Error bars show mean±SEM from n=3 independent experiments unless otherwise indicated. P-values were obtained using two-tailed unpaired Student's t-test as all comparisons were between two groups - control and experimental. Western blots and immunofluorescence images are representatives from least 3 independent experiments unless otherwise indicated.

Supplementary Material

Refer to Web version on PubMed Central for supplementary material.

Acknowledgments

This work was supported by grants from the National Institutes of Health (RO1GM111350-01 to M.O.), the National Cancer Institute (PO1 CA104838 to C.B.T., and the MSK Cancer Center Support Grant P30 CA008748), and the Benjamin Friedman Research Fund (M.O). W.P. is a recipient of the Genentech Foundation Hope Funds for Cancer Research Fellowship. The authors thank members of the Overholtzer laboratory for helpful suggestions. C.B.T. is a founder of Agios Pharmaceuticals and a member of its scientific advisory board. C.B.T. also serves on the board of directors of Merck.

References

Bridges D, Ma JT, Park S, Inoki K, Weisman LS, Saltiel AR. Phosphatidylinositol 3,5-bisphosphate plays a role in the activation and subcellular localization of mechanistic target of rapamycin 1. Molecular biology of the cell. 2012; 23:2955–2962. [PubMed: 22696681]

Burakoff R, Barish CF, Riff D, Pruitt R, Chey WY, Farraye FA, Shafran I, Katz S, Krone CL, Vander Vliet M, et al. A phase 1/2A trial of STA 5326, an oral interleukin-12/23 inhibitor, in patients with active moderate to severe Crohn's disease. Inflammatory bowel diseases. 2006; 12:558–565. [PubMed: 16804392]

Cai X, Xu Y, Cheung AK, Tomlinson RC, Alcazar-Roman A, Murphy L, Billich A, Zhang B, Feng Y, Klumpp M, et al. PIKfyve, a class III PI kinase, is the target of the small molecular IL-12/IL-23 inhibitor apilimod and a player in Toll-like receptor signaling. Chemistry & biology. 2013; 20:912–921. [PubMed: 23890009]

Commisso C, Davidson SM, Soydaner-Azeloglu RG, Parker SJ, Kamphorst JJ, Hackett S, Grabocka E, Nofal M, Drebin JA, Thompson CB, et al. Macropinocytosis of protein is an amino acid supply route in Ras-transformed cells. Nature. 2013; 497:633–637. [PubMed: 23665962]

Dayam RM, Saric A, Shilliday RE, Botelho RJ. The Phosphoinositide-Gated Lysosomal Ca Channel, TRPML1, Is Required for Phagosome Maturation. Traffic. 2015

de Lartigue J, Polson H, Feldman M, Shokat K, Tooze SA, Urbe S, Clague MJ. PIKfyve regulation of endosome-linked pathways. Traffic. 2009; 10:883–893. [PubMed: 19582903]

Descloux C, Ginet V, Clarke PG, Puyal J, Truttmann AC. Neuronal death after perinatal cerebral hypoxia-ischemia: Focus on autophagy-mediated cell death. International journal of developmental neuroscience : the official journal of the International Society for Developmental Neuroscience. 2015

Dong XP, Shen D, Wang X, Dawson T, Li X, Zhang Q, Cheng X, Zhang Y, Weisman LS, Delling M, et al. PI(3,5)P(2) controls membrane trafficking by direct activation of mucolipin Ca(2+) release channels in the endolysosome. Nature communications. 2010; 1:38.

Fairn GD, Grinstein S. How nascent phagosomes mature to become phagolysosomes. Trends in immunology. 2012; 33:397–405. [PubMed: 22560866]

Florey O, Gammoh N, Kim SE, Jiang X, Overholtzer M. V-ATPase and osmotic imbalances activate endolysosomal LC3 lipidation. Autophagy. 2015; 11:88–99. [PubMed: 25484071]

Florey O, Kim SE, Sandoval CP, Haynes CM, Overholtzer M. Autophagy machinery mediates macroendocytic processing and entotic cell death by targeting single membranes. Nature cell biology. 2011; 13:1335–1343. [PubMed: 22002674]

Garrity AG, Wang W, Collier CM, Levey SA, Gao Q, Xu H. The endoplasmic reticulum, not the pH gradient, drives calcium refilling of lysosomes. Elife. 2016; 5

Green RA, Kao HL, Audhya A, Arur S, Mayers JR, Fridolfsson HN, Schulman M, Schloissnig S, Niessen S, Laband K, et al. A high-resolution C. elegans essential gene network based on phenotypic profiling of a complex tissue. Cell. 2011; 145:470–482. [PubMed: 21529718]

Guan X, Qian Y, Shen Y, Zhang L, Du Y, Dai H, Qian J, Yan Y. Autophagy protects renal tubular cells against ischemia / reperfusion injury in a time-dependent manner. Cellular physiology and biochemistry : international journal of experimental cellular physiology, biochemistry, and pharmacology. 2015; 36:285–298.

Guo JY, Chen HY, Mathew R, Fan J, Strohecker AM, Karsli-Uzunbas G, Kamphorst JJ, Chen G, Lemons JM, Karantza V, et al. Activated Ras requires autophagy to maintain oxidative metabolism and tumorigenesis. Genes & development. 2011; 25:460–470. [PubMed: 21317241]

Gupta PD, Waheed AA. Effect of starvation on glucose transport and membrane fluidity in rat intestinal epithelial cells. FEBS letters. 1992; 300:263–267. [PubMed: 1555654]

He C, Klionsky DJ. Regulation mechanisms and signaling pathways of autophagy. Annual review of genetics. 2009; 43:67–93.

Hidalgo M. Pancreatic cancer. The New England journal of medicine. 2010; 362:1605–1617. [PubMed: 20427809]

Ho CY, Choy CH, Wattson CA, Johnson DE, Botelho RJ. The Fab1/PIKfyve phosphoinositide phosphate kinase is not necessary to maintain the pH of lysosomes and of the yeast vacuole. The Journal of biological chemistry. 2015; 290:9919–9928. [PubMed: 25713145]

Ikonomov OC, Sbrissa D, Shisheva A. Mammalian cell morphology and endocytic membrane homeostasis require enzymatically active phosphoinositide 5-kinase PIKfyve. The Journal of biological chemistry. 2001; 276:26141–26147. [PubMed: 11285266]

Ikonomov OC, Sbrissa D, Shisheva A. Localized PtdIns 3,5-P2 synthesis to regulate early endosome dynamics and fusion. American journal of physiology Cell physiology. 2006; 291:C393–C404. [PubMed: 16510848]

Jefferies HB, Cooke FT, Jat P, Boucheron C, Koizumi T, Hayakawa M, Kaizawa H, Ohishi T, Workman P, Waterfield MD, et al. A selective PIKfyve inhibitor blocks PtdIns(3,5)P(2) production and disrupts endomembrane transport and retroviral budding. EMBO reports. 2008; 9:164–170. [PubMed: 18188180]

Kamphorst JJ, Cross JR, Fan J, de Stanchina E, Mathew R, White EP, Thompson CB, Rabinowitz JD. Hypoxic and Ras-transformed cells support growth by scavenging unsaturated fatty acids from lysophospholipids. Proceedings of the National Academy of Sciences of the United States of America. 2013; 110:8882–8887. [PubMed: 23671091]

Kerr MC, Wang JT, Castro NA, Hamilton NA, Town L, Brown DL, Meunier FA, Brown NF, Stow JL, Teasdale RD. Inhibition of the PtdIns(5) kinase PIKfyve disrupts intracellular replication of Salmonella. The EMBO journal. 2010; 29:1331–1347. [PubMed: 20300065]

Kim GH, Dayam RM, Prashar A, Terebiznik M, Botelho RJ. PIKfyve inhibition interferes with phagosome and endosome maturation in macrophages. Traffic. 2014; 15:1143–1163. [PubMed: 25041080]

Kinchen JM, Ravichandran KS. Phagosome maturation: going through the acid test. Nature reviews Molecular cell biology. 2008; 9:781–795. [PubMed: 18813294]

Krajcovic M, Krishna S, Akkari L, Joyce JA, Overholtzer M. mTOR regulates phagosome and entotic vacuole fission. Molecular biology of the cell. 2013; 24:3736–3745. [PubMed: 24088573]

Krausz S, Boumans MJ, Gerlag DM, Lufkin J, van Kuijk AW, Bakker A, de Boer M, Lodde BM, Reedquist KA, Jacobson EW, et al. Brief report: a phase IIa, randomized, double-blind, placebo-

controlled trial of apilimod mesylate, an interleukin-12/interleukin-23 inhibitor, in patients with rheumatoid arthritis. Arthritis and rheumatism. 2012; 64:1750–1755. [PubMed: 22170479]

Lee JH, McBrayer MK, Wolfe DM, Haslett LJ, Kumar A, Sato Y, Lie PP, Mohan P, Coffey EE, Kompella U, et al. Presenilin 1 Maintains Lysosomal Ca(2+) Homeostasis via TRPML1 by Regulating vATPase-Mediated Lysosome Acidification. Cell reports. 2015; 12:1430–1444. [PubMed: 26299959]

Lito P, Saborowski A, Yue J, Solomon M, Joseph E, Gadal S, Saborowski M, Kastenhuber E, Fellmann C, Ohara K, et al. Disruption of CRAF-mediated MEK activation is required for effective MEK inhibition in KRAS mutant tumors. Cancer cell. 2014; 25:697–710. [PubMed: 24746704]

Mancias JD, Kimmelman AC. Targeting autophagy addiction in cancer. Oncotarget. 2011; 2:1302–1306. [PubMed: 22185891]

Matsui Y, Takagi H, Qu X, Abdellatif M, Sakoda H, Asano T, Levine B, Sadoshima J. Distinct roles of autophagy in the heart during ischemia and reperfusion: roles of AMP-activated protein kinase and Beclin 1 in mediating autophagy. Circulation research. 2007; 100:914–922. [PubMed: 17332429]

McNally K, Audhya A, Oegema K, McNally FJ. Katanin controls mitotic and meiotic spindle length. The Journal of cell biology. 2006; 175:881–891. [PubMed: 17178907]

Nicot AS, Fares H, Payrastre B, Chisholm AD, Labouesse M, Laporte J. The phosphoinositide kinase PIKfyve/Fab1p regulates terminal lysosome maturation in Caenorhabditis elegans. Molecular biology of the cell. 2006; 17:3062–3074. [PubMed: 16801682]

Overholtzer M, Mailleux AA, Mouneimne G, Normand G, Schnitt SJ, King RW, Cibas ES, Brugge JS. A nonapoptotic cell death process, entosis, that occurs by cell-in-cell invasion. Cell. 2007; 131:966–979. [PubMed: 18045538]

Palm W, Park Y, Wright K, Pavlova NN, Tuveson DA, Thompson CB. The Utilization of Extracellular Proteins as Nutrients Is Suppressed by mTORC1. Cell. 2015; 162:259–270. [PubMed: 26144316]

Racoosin EL, Swanson JA. Macropinosome maturation and fusion with tubular lysosomes in macrophages. The Journal of cell biology. 1993; 121:1011–1020. [PubMed: 8099075]

Rudge SA, Anderson DM, Emr SD. Vacuole size control: regulation of PtdIns(3,5)P2 levels by the vacuole-associated Vac14-Fig4 complex, a PtdIns(3,5)P2-specific phosphatase. Molecular biology of the cell. 2004; 15:24–36. [PubMed: 14528018]

Rusten TE, Rodahl LM, Pattni K, Englund C, Samakovlis C, Dove S, Brech A, Stenmark H. Fab1 phosphatidylinositol 3-phosphate 5-kinase controls trafficking but not silencing of endocytosed receptors. Molecular biology of the cell. 2006; 17:3989–4001. [PubMed: 16837550]

Samie M, Wang X, Zhang X, Goschka A, Li X, Cheng X, Gregg E, Azar M, Zhuo Y, Garrity AG, et al. A TRP channel in the lysosome regulates large particle phagocytosis via focal exocytosis. Developmental cell. 2013; 26:511–524. [PubMed: 23993788]

Sbrissa D, Ikonomov OC, Fu Z, Ijuin T, Gruenberg J, Takenawa T, Shisheva A. Core protein machinery for mammalian phosphatidylinositol 3,5-bisphosphate synthesis and turnover that regulates the progression of endosomal transport. Novel Sac phosphatase joins the ArPIKfyve-PIKfyve complex. The Journal of biological chemistry. 2007; 282:23878–23891. [PubMed: 17556371]

Sbrissa D, Ikonomov OC, Shisheva A. PIKfyve, a mammalian ortholog of yeast Fab1p lipid kinase, synthesizes 5-phosphoinositides. Effect of insulin. The Journal of biological chemistry. 1999; 274:21589–21597. [PubMed: 10419465]

Shisheva A. PIKfyve: the road to PtdIns 5-P and PtdIns 3,5-P(2). Cell biology international. 2001; 25:1201–1206. [PubMed: 11748912]

Sun M, Goldin E, Stahl S, Falardeau JL, Kennedy JC, Acierno JS Jr, Bove C, Kaneski CR, Nagle J, Bromley MC, et al. Mucolipidosis type IV is caused by mutations in a gene encoding a novel transient receptor potential channel. Human molecular genetics. 2000; 9:2471–2478. [PubMed: 11030752]

Wong CO, Li R, Montell C, Venkatachalam K. Drosophila TRPML is required for TORC1 activation. Current biology : CB. 2012; 22:1616–1621. [PubMed: 22863314]

Yang S, Wang X, Contino G, Liesa M, Sahin E, Ying H, Bause A, Li Y, Stommel JM, Dell'antonio G, et al. Pancreatic cancers require autophagy for tumor growth. Genes & development. 2011; 25:717–729. [PubMed: 21406549]

Highlights

- PIKfyve regulates vacuole shrinkage and cargo redistribution during engulfment
- Vacuole shrinkage is controlled in part through downstream PIKfyve effector TRPML1
- PIKfyve activity promotes the export of nutrients from vacuoles
- PIKfyve-dependent nutrient export supports growth of engulfing cells during starvation

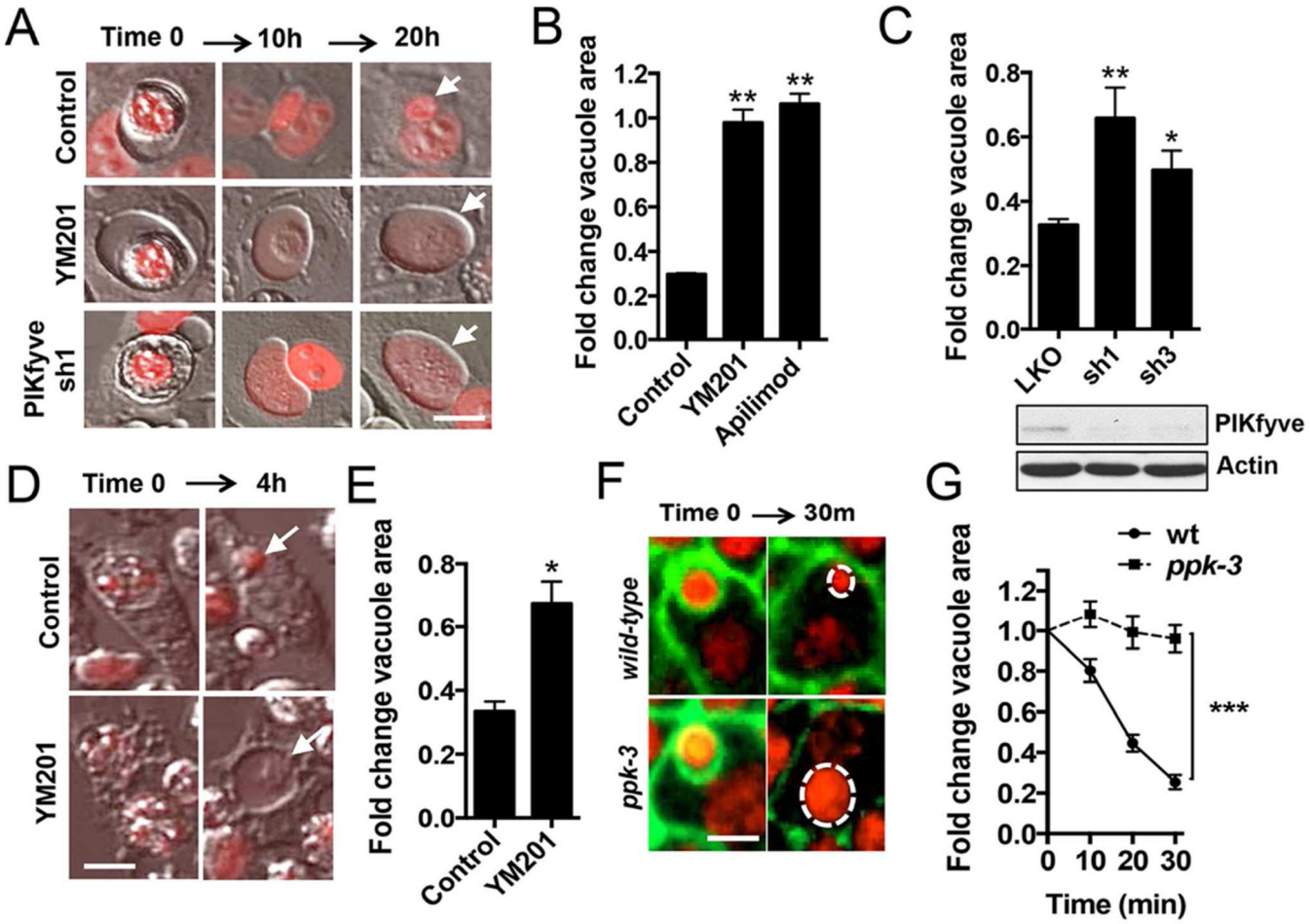

Figure 1. PIKfyve regulates entotic vacuole and phagosome shrinkage *in vitro* and *in vivo*

A) Entotic vacuoles in MCF10A cells undergo PIKfyve-dependent shrinkage. Images show representative entotic vacuoles containing engulfed cell corpses in control and PIKfyve-inhibited cells (YM201 treatment, middle panels; shRNA knockdown, bottom panels). Note that vacuoles in PIKfyve-inhibited cells fail to shrink over 20 hours despite the degradation of cell corpses (arrows). See Supplementary Movie S1. B) Treatment with PIKfyve inhibitors (YM201 and Apilimod) delays entotic vacuole shrinkage. Graph shows fold change in area of entotic vacuoles after 10 hours determined by time-lapse microscopy, for control and PIKfyve-inhibited cells. Total cell number analysed for control n=168, YM201 n=119, Apilimod n=86. C) shRNA-mediated PIKfyve knockdowns delay entotic vacuole shrinkage in MCF10A cells. Graph shows quantification of vacuole shrinkage after 10 hours, western blot shows PIKfyve expression in control and knockdown cells. Total cell number analysed for LKO n=131, sh1 n=56, sh3 n=84. D) Apoptotic cell phagosomes undergo PIKfyve-dependent shrinkage in macrophages. Images show representative apoptotic cell phagosomes in control and PIKfyve-inhibited J774.1 mouse macrophages. Note that the PIKfyve-inhibited phagosome (bottom panel, arrow) fails to shrink over 4 hours despite degradation of the engulfed apoptotic corpse. E) Treatment of J774.1 macrophages with the PIKfyve inhibitor YM201 delays apoptotic phagosome shrinkage. Graph shows fold change in area of phagosomes after 4 hours. Total cell number analysed

for Control n=103, YM201 n=92. F) *ppk3* (PIKfyve ortholog) controls phagosome shrinkage during *C. elegans* development. Images show H2B-mCherry and PIP2-GFP fluorescence during apoptotic cell phagocytosis. Note that the *wild-type* phagosome (top panel, circle) undergoes rapid shrinkage while the phagosome in a *ppk3* mutant embryo (bottom panel, circle) shows delayed shrinkage. G) Quantification of fold change in area of apoptotic phagosomes, 30 minutes after engulfment in *wild-type* and *ppk3* mutant C. *elegans* embryos, as determined by time-lapse microscopy. Error bars show mean±SEM for n=7 embryos. For all graphs, error bars show mean±SEM for n=3 independent experiments unless otherwise mentioned. *p<0.05, **p<0.02 (Student's t-test). Scale bars equal 10μm. See supplemental Figures S1 and S2.

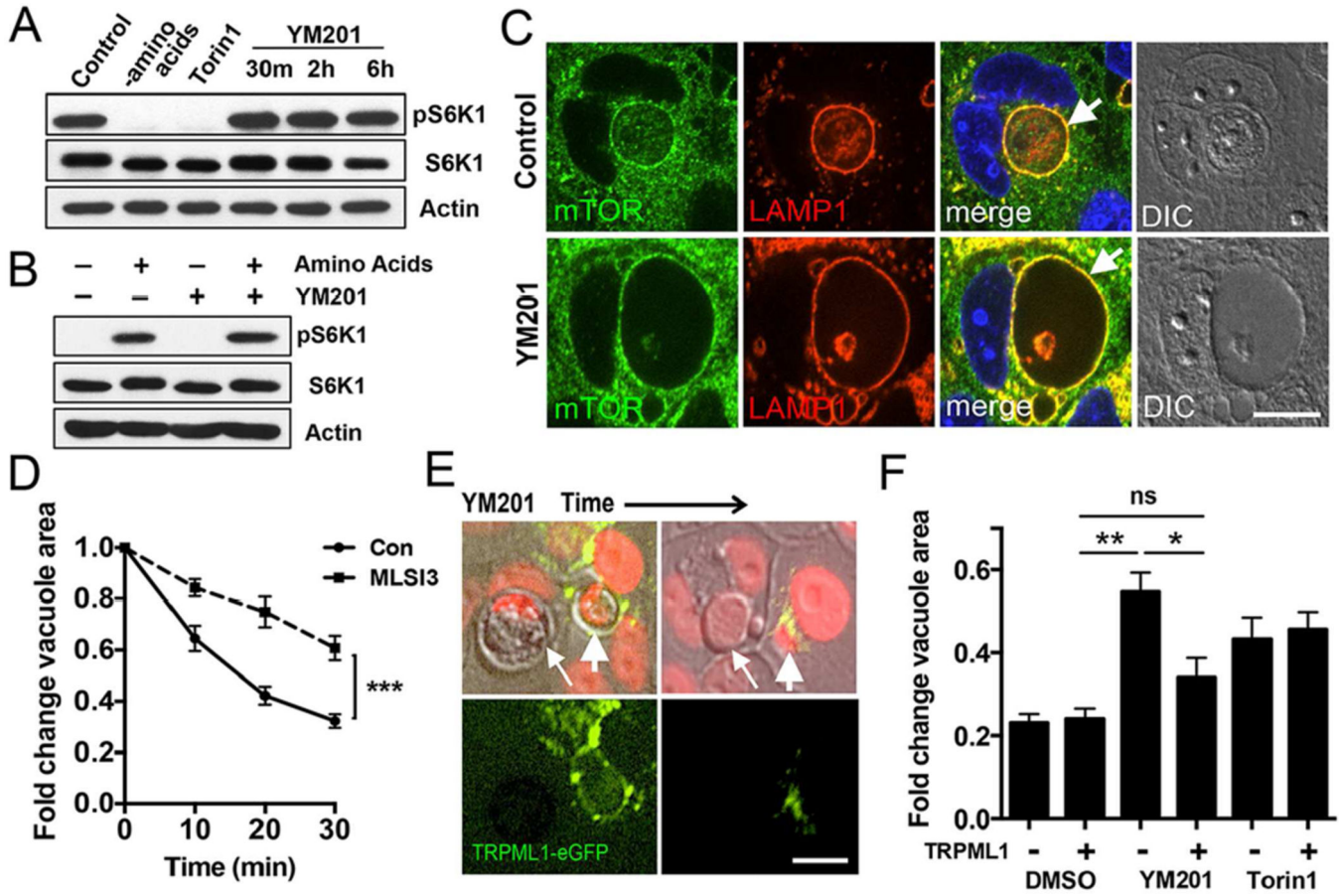

Figure 2. PIKfyve regulates vacuole shrinkage through TRPML1 in an mTORCI-independent manner

A) mTORC1 activity in cells cultured in full media is not affected by PIKfyve inhibition. Western blot of MCF10A cell lysates shows phosphorylation of the mTORC1 target S6-kinase threonine 389 (pS6K) in full media (Control), amino-acid starved, Torin1-treated, and YM201-treated conditions, as indicated. PIKfyve inhibition by YM201 treatment for 30 minutes, 2 hours or 6 hours does not affect pS6K levels. B) mTORC1 stimulation by amino acids is not affected by PIKfyve inhibition. Western blot shows pS6K levels in amino acid-starved and restimulated MCF10A cells in the presence and absence of YM201. C) mTOR localization onto entotic vacuoles in MCF10A cells is not affected by PIKfyve inhibition. Top, mTOR (green) is recruited to a corpse-containing entotic vacuole (arrow), where it colocalizes with Lamp1 (red). Bottom, treatment with the PIKfyve inhibitor YM201 for 18 hours does not inhibit mTOR colocalization with Lamp1 on entotic vacuole (arrow). Panels show confocal microscopic imaging of immunofluorescence staining. D) TRPML1 inhibitor ML-SI3 delays macropinosome shrinkage in J774.1 macrophage cells. Graph shows fold change in area of macropinosomes after 30min.Total cell number analysed for Control n=12, ML-SI3 n=15. E) TRPML1 overexpression rescues entotic vacuole shrinkage in PIKfyve-inhibited MCF10A cells (YM201 0.2μM). Note that entotic vacuole in TRPML1-eGFP-expressing cell (green, right arrow) shrinks rapidly while control vacuole in adjacent, non-expressing cell (left arrow) fails to shrink as corpse is degraded. See Supplementary Movie S4. F) TRPML1-eGFP overexpression rescues entotic vacuole shrinkage in PIKfyve-

inhibited (YM201 0.2μM), but not mTOR-inhibted (Torin1 1μM), MCF10A cells. Graph shows fold change in vacuole area after 20 hours for control, PIKfyve and mTOR-inhibited MCF10A cells, with or without TRPML1-eGFP expression as measured by time-lapse microscopy. Total cell number DMSO TRPML1 Neg n=78, DMSO TRPML1 Pos n=72, YM201 TRPML1 Neg n=60, YM201 TRPML1 Pos n=42, Torin TRPML1 Neg n=50, Torin TRPML1 Pos n=39. For all graphs, error bars show mean±SEM for n=3 independent experiments, *$p<0.05$, **$p<0.02$ (Student's t-test). Scale bars equal 10μm. See supplemental Figure S3.

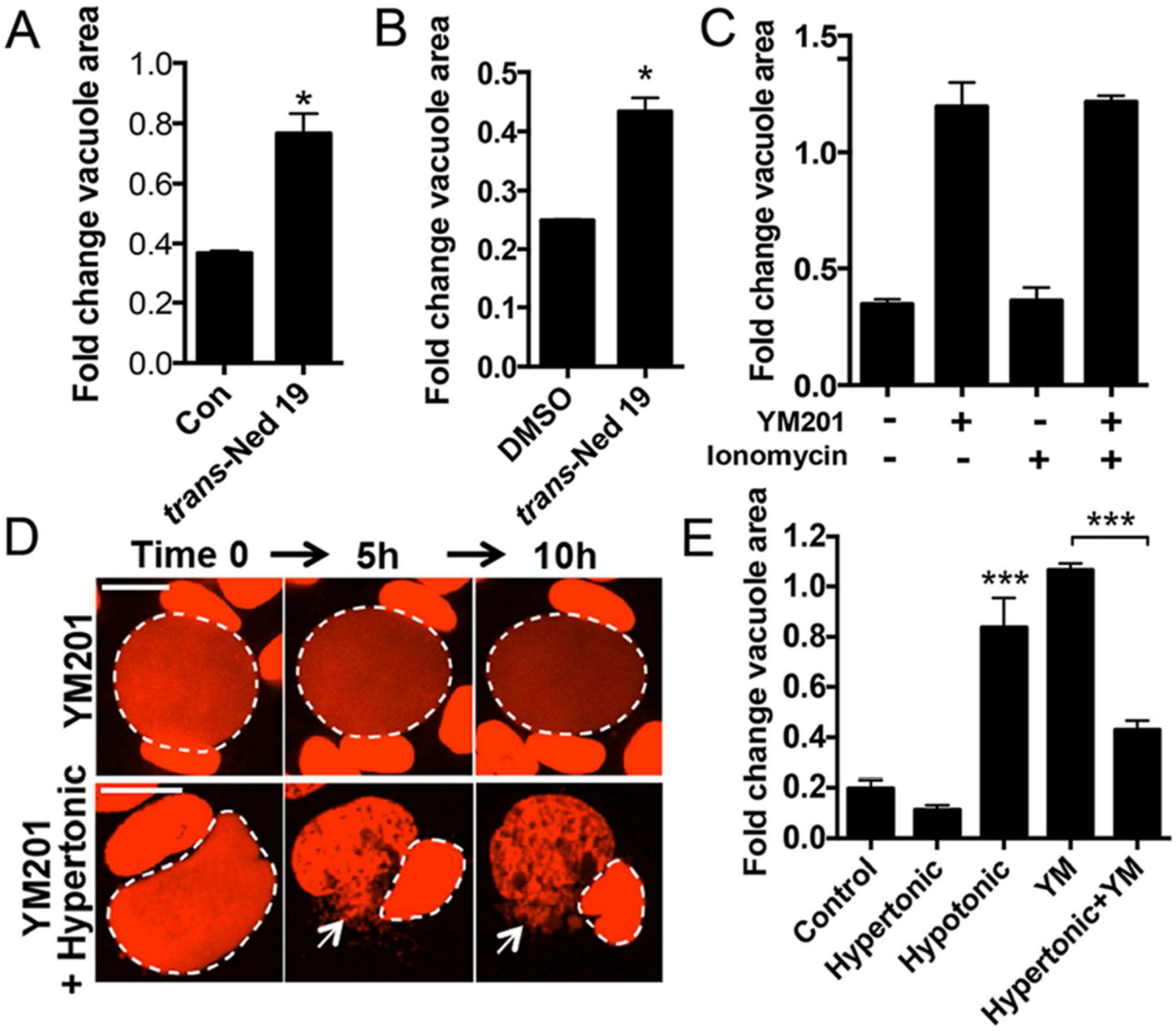

Figure 3. Lysosomal cation fluxes regulate vacuole fission downstream of PIKfyve

A) Treatment of MCF10A cells with *trans*-Ned 19 delays entotic vacuole shrinkage. Graph shows fold change in area of entotic vacuoles after 10 hours. Total cell number control n=81 *trans*-Ned 19 n=85. B) Treatment of MCF10A cells with *trans*-Ned 19 delays shrinkage of vacuoles resulting from pre-treatment with PIKfyve inhibitor YM201. Graph shows fold change in area of vacuoles pre-treated with YM201, and then subjected to YM201 washout and treatment with vehicle control or *trans*-Ned 19 for 10 hours. Total cell number Control n=96, *trans*-Ned 19 n=90. C) Treatment with Ionomycin does not rescue effects of PIKfyve inhibition on vacuole fission. Graphs show fold change in area of vacuoles treated with YM201 with or without Ionomycin. Total cell number Control n=32 ,YM n=38, Ionomycin n=30, Ionomycin+YM n=30. D) Treatment with hypertonic medium rescues the effects of PIKfyve inhibition. Vacuoles generated from YM201 pre-treatment in MCF10A cells do not undergo shrinkage in YM201 full media conditions (top panel, circle), but undergo rapid

shrinkage and fission in YM201 with hypertonic media (bottom panel, circle) with mCherry vesicles accumulating in the cytosol (arrow) See Supplementary Movie S5. E) Graph shows fold change in area of vacuoles pre-treated with YM201, and then subjected to hypertonic or hypotonic medium for 10 hours. Total cell number Control n=41, Hypertonic n=39, Hypotonic n=35, YM n=35, Hypertonic +YM n=39. For all graphs, error bars show mean ±SEM for n=3 independent experiments, *$p<0.05$, **$p<0.02$ (Student's t-test). See supplemental Figure S5.

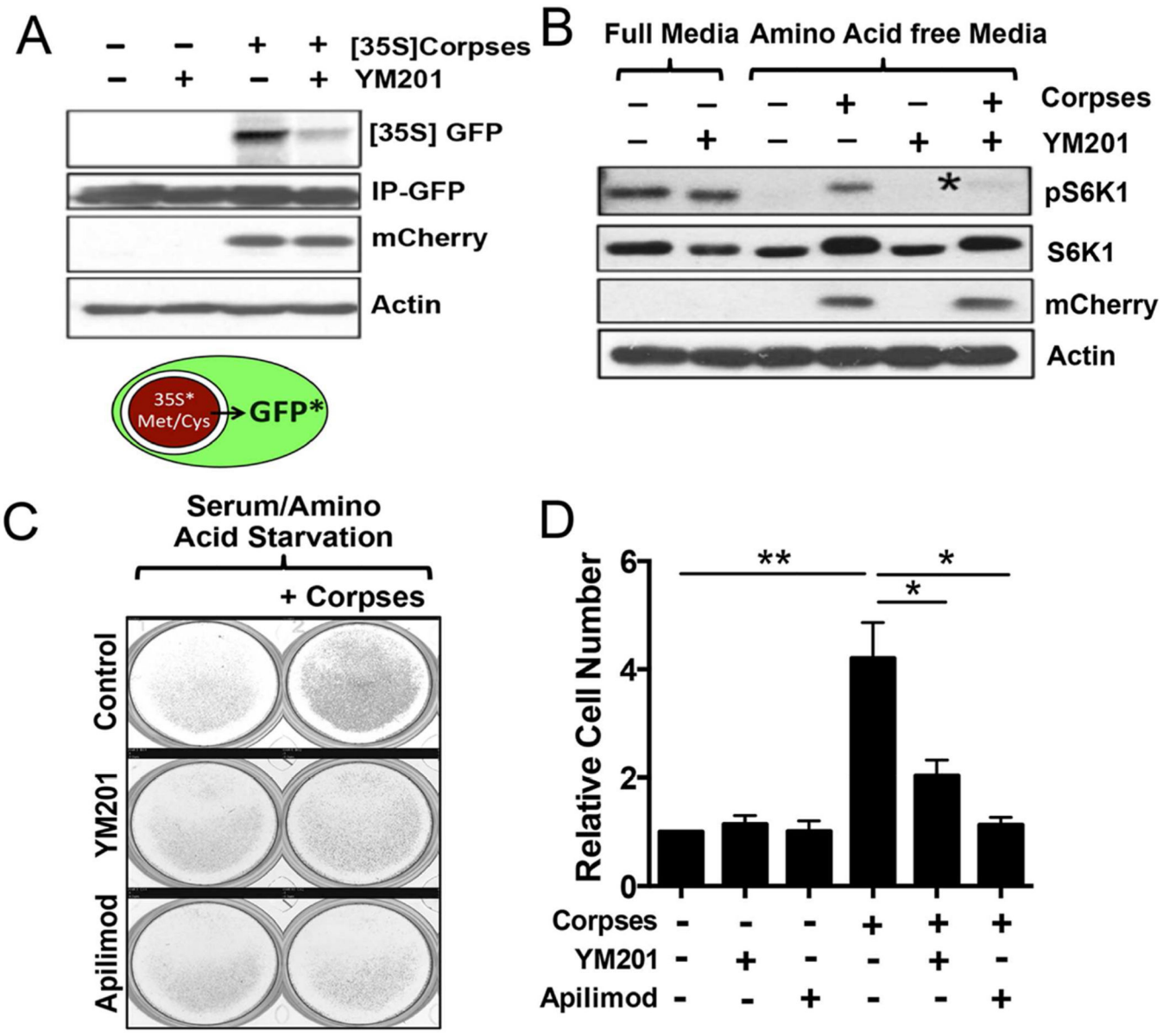

Figure 4. PIKfyve-mediated maturation regulates nutrient recovery from phagosomes

A) PIKfyve inhibition blocks amino acids efflux from phagosomes. Blot shows 35S-cysteine and methionine incorporation into macrophage-expressed GFP (top lane), following phagocytosis of H2B-mCherry expressing apoptotic corpses. Note that PIKfyve inhibition reduces levels of radiolabeled GFP, but does not affect the engulfment and degradation marked by the presence of free mCherry. Cartoon shows a schematic of the radiolabeled amino acid incorporation into GFP. B) mTORCI reactivation by apoptotic corpse engulfment is blocked by PIKfyve inhibition. Western blot shows pS6K phosphorylation in J774.1 macrophages cultured in full or amino acid-free media, in the presence or absence of apoptotic corpses and the PIKfyve inhibitor YM201. Note that the loss of pS6K in amino acid-starved cells is rescued by apoptotic corpses (lane 4), and this rescue is blocked by PIKfyve inhibition (lane 6, asterisk). C) Rescue of macrophage proliferation during

starvation by apoptotic cell engulfment is blocked by PIKfyve inhibition. Images show representative crystal violet-stained J774.1 macrophage cultures in serum/amino acid-free media, in the presence or absence of apoptotic corpses and 2μM YM201 or 0.1μM Apilimod. D) Fold change in cell number of J774.1 macrophages cultured in serum/amino acid starvation media, with or without the indicated PIKfyve inhibitors, and in the presence or absence of apoptotic corpses. For all graphs, error bars show mean±SEM for n=3 independent experiments, *$p<0.05$, **$p<0.02$ (Student's t-test). See supplemental Figure S5.

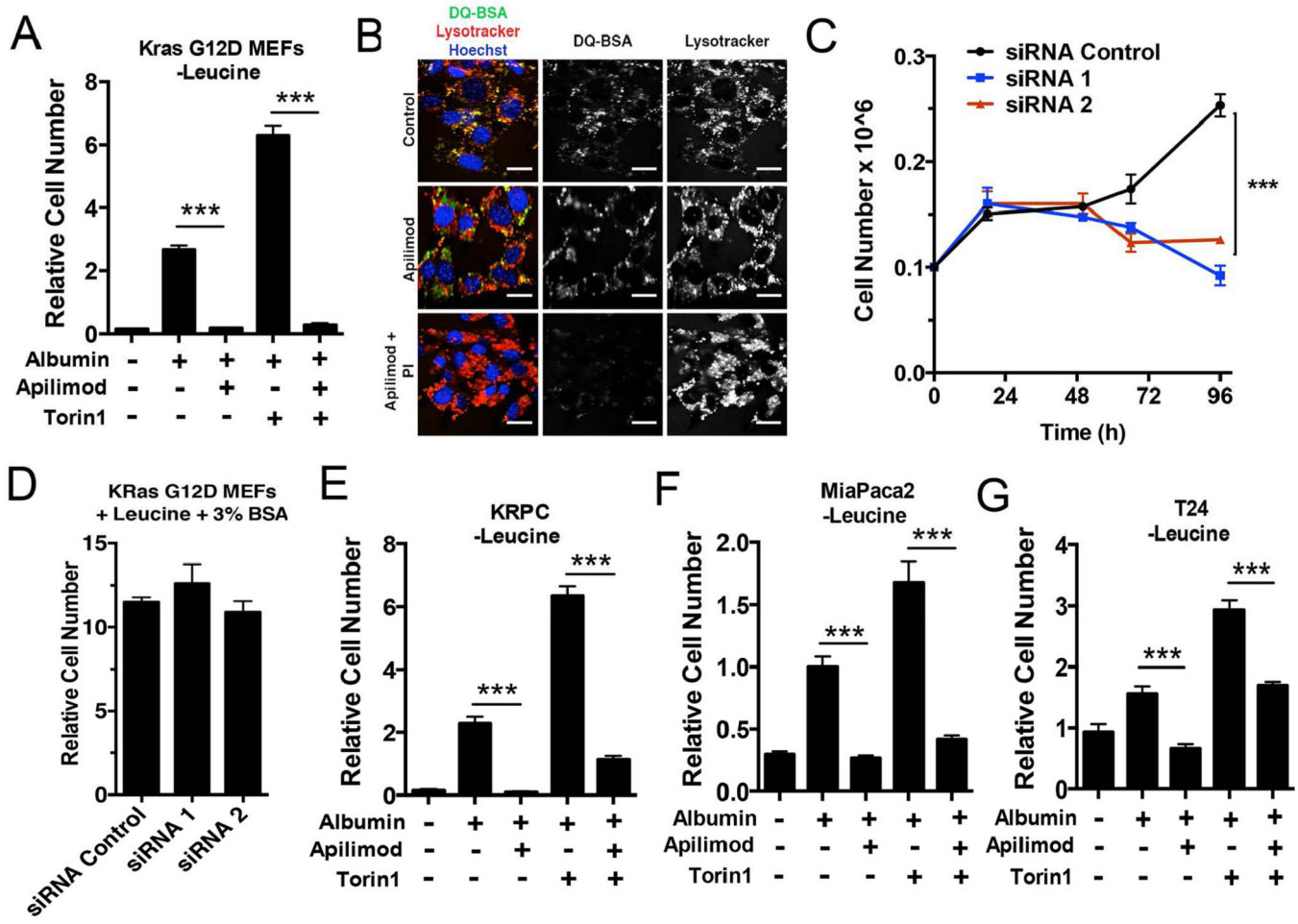

Figure 5. PIKfyve regulates albumin-dependent growth of Ras-transformed cells

A) Rescue of leucine-starved Kras G12D MEF cell growth by engulfment of albumin requires PIKfyve activity. Graph shows relative change in cell number in leucine-free conditions from day 0 to day 4 in the presence or absence of 3% albumin supplementation, and treatment with Apilimod or Torin1. Note that treatment with the PIKfyve inhibitors Apilimod and YM201 abolished the BSA-dependent rescue of cell proliferation and the Torin1-dependent increase in cell proliferation during leucine deprivation. B) PIKfyve inhibition does not affect lysotracker staining or BSA degradation in Kras G12D MEFs. Images show merge of lysotracker and DQ-BSA fluorescence (top left), and individual DQ-BSA (top center) and lysotracker (top right) fluorescence channels in control, Apilimod-treated, and Apilimod plus protease inhibitor (Pi)-treated Kras G12D MEFs. C) siRNA-mediated PIKfyve knockdowns inhibit albumin-dependent growth of leucine-starved Kras G12D MEFs. Graph shows relative change in cell number in leucine-free conditions from day 0 to day 4 with albumin supplementation. D) siRNA-mediated PIKfyve knockdowns do not affect the growth of Kras G12D MEF cells in full media conditions. Graphs show relative change in cell number in leucine-replete media from day 0 to day 2 with albumin supplementation. E) Rescue of leucine-starved Kras mutant tumor cell growth by engulfment of albumin requires PIKfyve activity. Graph shows relative change in cell number in leucine-free conditions from day 0 to day 4 for the indicated cell lines: E) KRPCs

F) MiaPaca2 and G) T24. Apilimod was used at 0.1μM for Kras G12D MEFs and at 0.6μM for KRPC, MiaPaca2 and T24 cells. All Graphs show representative data from one of three independent experiments, error bars show mean±SD, ***$p<0.01$. Scale bars equal 10μm. See supplemental Figure S4.